Pattern dynamics in a perturbed printer's instability experiment

R. L. Santos,* U. Agero, and J. M. A. Figueiredo†
Departamento de Física, Universidade Federal de Minas Gerais, Caixa Postal 702, Belo Horizonte, CEP 31.270-901, Brazil
(Received 31 August 2007; revised manuscript received 13 February 2008; published 19 June 2008)

We report experimental results concerning observation of a pattern forming system, subject to directional viscous fingering (printer's instability). This system was excited by a time-dependent, periodic perturbation. A variety of spatiotemporal effects was observed, including pattern transient dynamics, wave vector selection, and morphological transitions. Detailed measurement of pattern shape and its associated Fourier modes assured the detection of a crossover between different regimes of the pattern evolution.

DOI: 10.1103/PhysRevE.77.066310 PACS number(s): 47.54.−r, 47.20.Ky, 47.20.Hw, 05.70.Ln

I. INTRODUCTION

An important case of pattern formation in nonequilibrium thermodynamic systems refers to one-dimensional cellular patterns. Although this kind of structure presents an inherent simplicity, it exhibits a large variety of dynamical regimes as shown by Coullet and Iooss [1], who used symmetry arguments to report the existence of ten generic instabilities in one-dimensional periodic patterns. These structures are observed, for example, in a fluid-fluid interface subject to directional viscous fingering (DVF). Several configurations of actual systems fit this class of hydrodynamic model, being printing machines, in which a liquid is forced to flow into the gap between a rotating cylinder and a plate, a case in point. Instabilities in the liquid-air interface in this system were originally described by Pitts and Greiller [2] and by Taylor [3]. Pattern formation in a different configuration consisting of two eccentrical rotating cylinders was also reported by Rabaud *et al.* [4–6], who investigated some processes that may affect symmetry properties of the observed spatial patterns. Studies concerning the linear stability analysis of the DVF instability were performed by Hakim *et al.* [7]. Secondary instabilities were reported by Pan and Bruyn [8,9], Michalland *et al.* [10], and phase space domains were reported by Cummins *et al.* [11]. Michalland and Rabaud [12] also described the features of transition to chaos in DVF, and Fourtune *et al.* [13] demonstrated the existence of phase diffusion effects for this system. Time response of a system using the same configuration as in Ref. [7] was reported by Santos and Figueiredo [14], who excited the hydrodynamic fields of this system by an externally imposed periodic perturbation, whose effect on the interface position was observed, at both prebifurcation and postbifurcation regimes.

In this work we report studies on the dynamical properties of pattern formation in a DVF system, generated under the same experimental conditions used in Ref. [14]. We show that the imposed perturbation may affect the evolution of pattern modes and may persist even when there is a saturation of mode amplitudes. Our observations also indicate that pattern morphology is associated with the wave vector selection process. This work is organized as follows. In Sec. II we present the experimental setup, the range of parameters, and the kind of perturbation used in the experiments, as well as a brief discussion of precursor modes, already reported in Ref. [14]. Section III focuses on the mutual influence of pattern morphology and the precursor modes. In Sec. IV we present results concerning the evolution of spatial modes in both the transient and saturation regimes, and effects relating morphology and pattern selection dynamics.

II. EXPERIMENTAL SETUP

For this experiment, a cylindrical stainless steel shaft (with measured roughness ~ 1 μm), driven by a precision dc motor and mounted on aligned bearings, was designed. The cylinder rotates immersed in a flat reservoir containing silicon oil. Parallelism between the cylinder axis and the horizontal base of the reservoir is adjusted by supporting precision screws so as to ensure that there is a gap between this cylinder and the base. A sketch of the experimental setup is shown in Fig. 1. The cylinder is 250 mm long, has an average radius value (R_0) of 31.3 mm, and an eccentricity (ϵ) of $\simeq 10$ μm. As shown in Table I three different values for the mean gap distance (b_0) between the cylinder and the plate were adjusted: 300 μm, 400 μm, and 800 μm. This table also displays the range of angular frequencies (ω) of the

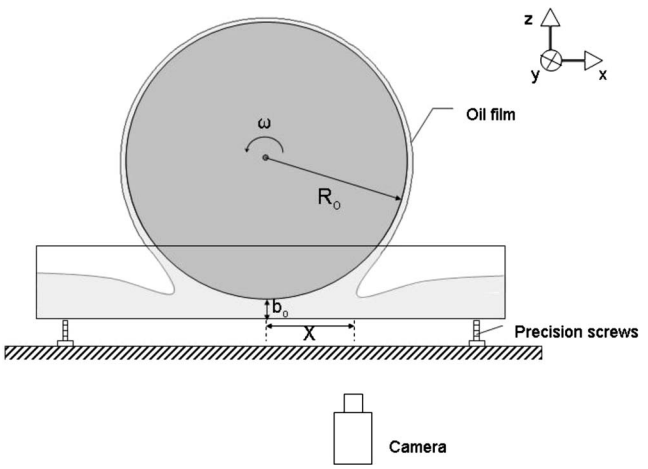

FIG. 1. Sketch of the experimental setup. The cylinder was adjusted at three distances to the plate, $b_0=300$ μm, $b_0=400$ μm, and $b_0=800$ μm.

*robson@fisica.ufmg.br
†josef@fisica.ufmg.br

TABLE I. Values of the parameters used in the experimental setup. Values of the critical velocity (ω_c) for each set of experiments are also shown.

Distance b_0 (μm)	Range of ω (rad s^{-1})	ω_c (rad s^{-1})
300	1.30–5.38	2.53
400	1.10–8.71	4.87
800	2.61–16.67	11.58

cylinder used in the experiments. Values of the critical angular frequency measured at the bifurcation are shown in the third column of this table.

Silicon oil (Dow Corning 200) with viscosity (μ) equal to 4.80×10^{-2} kg m^{-1} s^{-1} and surface tension (T) equal to 2.08×10^{-2} N m^{-1}, both specified at 25 °C, was used as the liquid fluid in our experiments. For better stability of these parameters, room temperature was constantly monitored within ±0.5 °C. Since the axis-to-base distance is constant, eccentricity introduces a time dependence on gap values given by

$$b(t) = b_0 - \epsilon \sin(\omega t), \tag{1}$$

which acts as an external perturbation imposed on the system.

A clear meniscus located at the oil-air (open atmosphere) interface was observed with a 648 (H)$\times$484 (V) asynchronous mode digital camera at a frame rate of 17 s^{-1} and a spatial resolution of 68 μm/pixel. As shown in Fig. 2 a high contrast image of the interface was obtained. Interface shape is depicted mostly as a thin strip, whose profile was obtained from a computer program we developed using edge detection techniques. Its output delivers, for a given horizontal position y (see Fig. 2), the coordinate $f(y)$ of maximum contrast. In order to follow the dynamics of the interface we have obtained, for each value of the mean distance b_0 and each adjusted angular frequency, a sequence of images. At the critical frequency ω_c the straight morphology becomes unstable and a bifurcation happens. The system shifts to a new morphological state presenting a periodic pattern as shown in the Fig. 2(b).

Interface data were treated using a numerical Fourier analysis. We did not make use of fast Fourier transform (FFT) algorithms in treating the spatial modes. We wrote our own Fourier transform routine (a discrete Fourier transform (DFT) algorithm [15]) in such a way that the diffraction of the observation window was taken into account. This way, to be consistent with uncertainty induced by this window, wave vector resolution was calculated with much more precision ($\delta k=0.025$ mm^{-1}) than that defined by the normal modes of the window (used in FFT algorithms). Afterwards we checked that Parseval's theorem was satisfied. As a final procedure, our routine was applied to standard monomode and multimode patterns, artificially generated with different amplitudes, and we checked again that its output was calibrated.

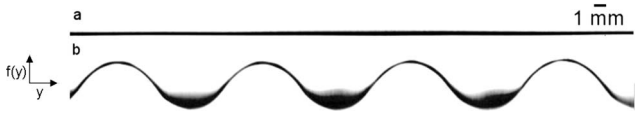

FIG. 2. Images of the straight (a) and periodic (b) morphologies of the interface. In both images the open atmosphere is located above the interface and silicon oil is located below the interface. Experiments set for $b_0=400$ μm and $\omega=4.85$ rad/s (a) and $\omega=5.39$ rad/s (b).

The range of angular frequencies of the rotating cylinder was chosen in order to get information concerning interface dynamics at both prebifurcation and postbifurcation regimes. For a better comparison of the different experiments we have defined a reduced control parameter for this system as

$$\xi \equiv \frac{\omega - \omega_c}{\omega_c}. \tag{2}$$

As the cylinder begins to turn, pressure and velocity fields are established in this system. Due to competitive forces between these fields and also to wetting and surface tension effects, the interface experiences a recoil. A steady hydrodynamic model was developed by Hakim *et al.* [7] that predicts the interface position x (see Fig. 1) in the straight morphology (the prebifurcation branch) as a function of the control parameter. As made in the previous work (Ref. [14]), we fit our recoil data to Eq. (10) of Ref. [7] in order to get parameters of the capillarity function F(Ca). In the present work, these values will be used when we compare our data of pattern growth rates to linear stability analysis predictions.

The existent eccentricity introduces a time-dependent variation on gap values as described by Eq. (1). Thus it is expected that recoil values should be influenced by this perturbation. In fact, we have observed [14] an oscillatory motion of the mean value of the interface profile $f(y)$. Amplitude values measured for the fundamental Fourier mode of these oscillations as a function of the control parameter are shown in Fig. 3. It confirmed the existence of this phenomenon in all the experiments performed, although it was less pronounced when the distance b_0 became larger. It is clear from these data that mode amplification is observed as the control parameter approaches zero (the bifurcation point). After this point, the amplitude of the oscillations, still measured as the mean interface profile, decreases to the low values observed at low velocities (larger negative control parameter). These results (Ref. [14]) showed that those amplified modes follow a power law in the prebifurcation branch and an exponential decreasing in the postbifurcation branch determining the existence of a cuspid at the bifurcation point. As discussed in Ref. [14], so far there is no simple explanation for these effects. It is evident, however, that they reveal the existence of a new phenomenon in this pattern-forming system, one that is not present in the unperturbed case. This kind of instability is known as a precursor. Its importance has been verified in other contexts as earthquakes [16,17] and epileptic seizures [18,19]. In fact, theoretical results found by Wiesenfeld [20], show the existence of bifurcations signaled by precursors. In the following sections we

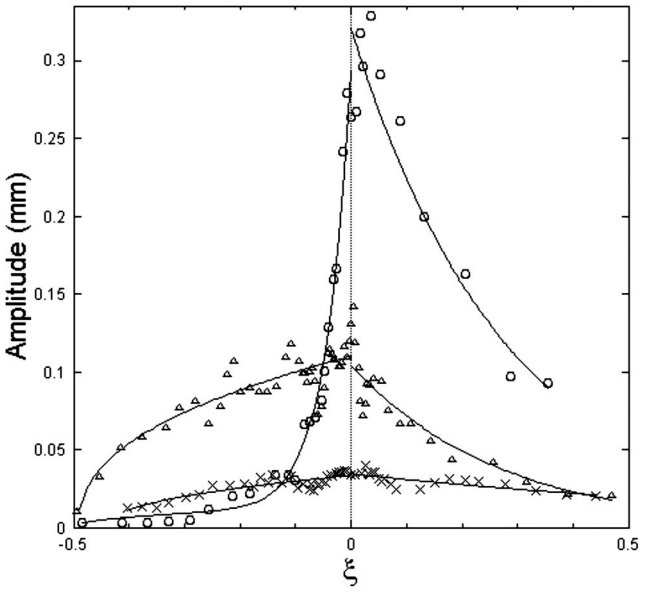

FIG. 3. Amplitude of the fundamental Fourier mode [(○) for b_0=300 μm, (△) for b_0=400 μm, and (×) for b_0=800 μm] adjusted to a power law in the prebifurcation branch and to an exponential in the postbifurcation branch (Ref. [14]).

report our observations concerning the effects of the perturbed interface on the emergence of pattern formation.

III. MORPHOLOGICAL EFFECTS IN THE POSTBIFURCATION BRANCH

At the bifurcation point, the highly symmetrical morphology of the straight interface spontaneously breaks into a periodic pattern. In our experiment, we were able to observe how the pattern evolved along all the stages of both transient and saturation regimes. In order to study this phenomenon, spatial modes of the interface profile were obtained from a numerical Fourier transform of those data, allowing spectra to be followed in time. Observation of these modes revealed that their amplitude oscillated with the same angular frequency as the cylinder. Time dependence of this amplitude and the mean interface position for a typical experiment is depicted in Fig. 4, which clearly shows that eccentricity affects the pattern formed. Close to the bifurcation, at low positive values of ξ, we observed oscillations with larger amplitude in pattern valley (small x in the Fig. 1) than in its crest. For larger values of ξ, these oscillations became more pronounced in crests than in valleys. It appears that this effect might be responsible for the observed suppression of the mean interface position oscillations displayed in the right side of Fig. 3.

In order to test this possibility, we made an inspection in the shape of the pattern as the control parameter varied. In fact, pattern morphology (see Fig. 5) has different aspects for each value of the control parameter. To do this, we first calculated the mean interface profile. This defines unambiguously valley and crest regions of the pattern. Then we got valley and crest widths measured at pattern half height. From these measurements, the pattern aspect ratio, defined as

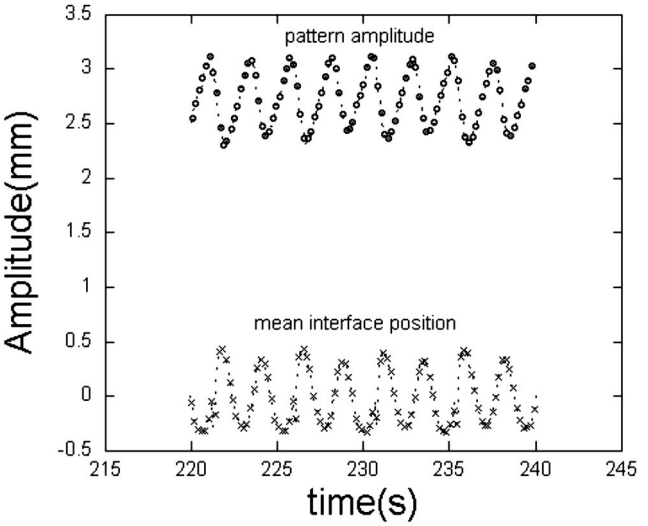

FIG. 4. Time response of this system subject to a deterministic perturbation. This picture shows time oscillations of pattern amplitude (upper) and mean interface position (lower) for an experiment adjusted for b_0=300 μm and ξ=0.05.

$$\Gamma = \frac{W_+ - W_-}{W_+ + W_-}, \tag{3}$$

was calculated. Here W_+ is the average crest width and W_- is the average valley width. These results are shown in Fig. 6, which displays the plotted values of Γ against the control parameter for all the distances b_0 used. In the same frame, peak values of the mean interface position oscillations are also shown. In the two most critical cases (b_0=300 μm and b_0=400 μm), a change in the sign of Γ was observed. In both cases, Γ is positive for low (positive) values of the control parameter, meaning that crest width is larger than valley width. For large enough values of the control parameter, close to ~0.10–0.20, Γ becomes negative. For the largest distance b_0, Γ is always negative regardless of the cylinder velocity. It was observed that the change in the character of pattern morphology (the sign of Γ) roughly coincides with the strong suppression of the oscillatory modes induced by the imposed time-dependent perturbation, thus confirming the existence of joint influence of these different phenomena.

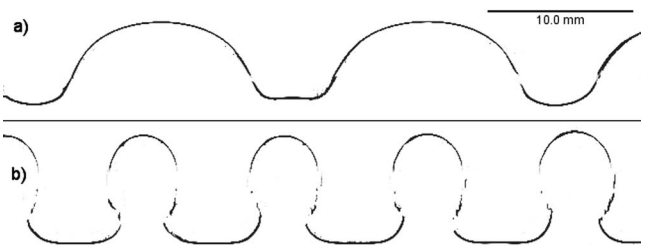

FIG. 5. The asymmetrical morphologies presented by periodic spatial patterns. In (a) is shown one pattern with a larger crest compared to its valley and in (b) is shown another pattern having a valley larger than its crest. Both pictures refer to b_0=300 μm and ξ=0.05 (a) and ξ=0.29 (b).

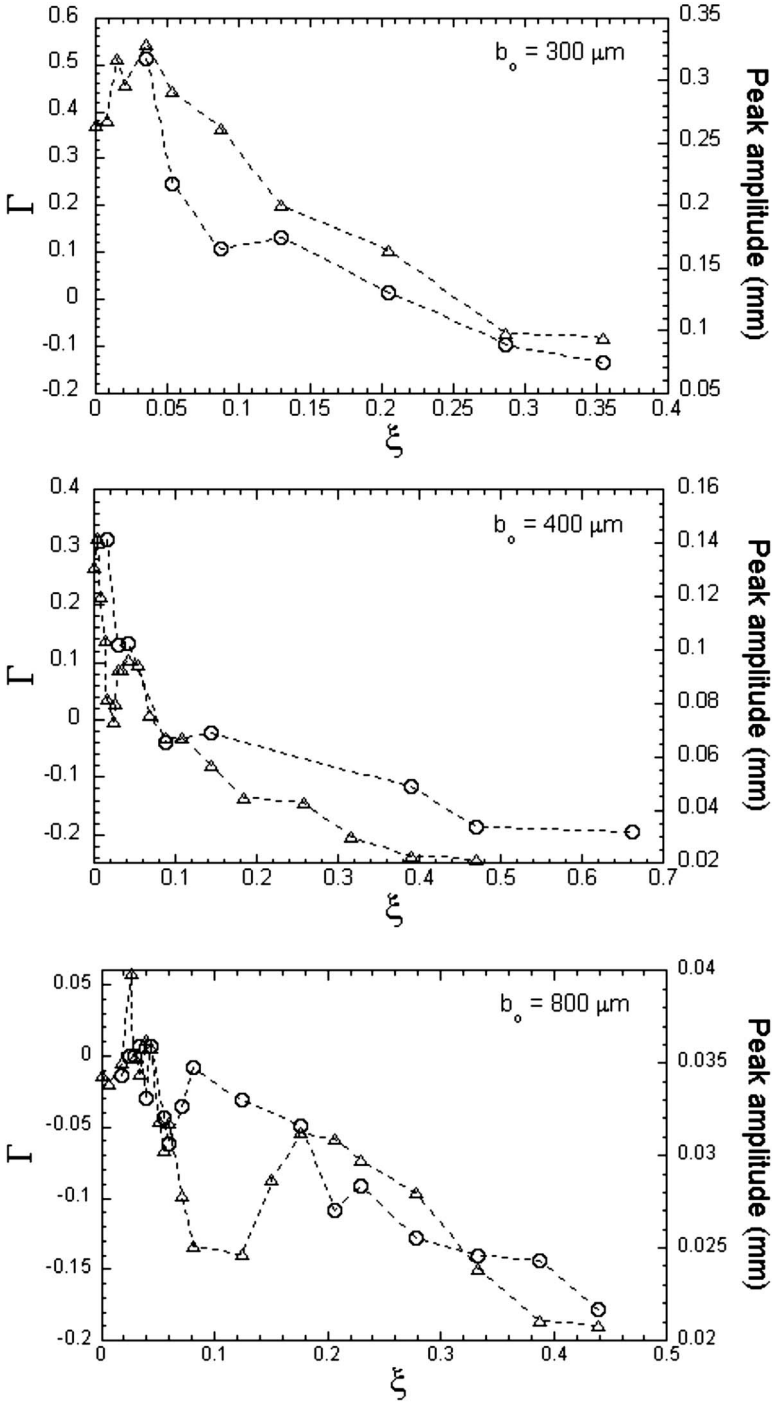

FIG. 6. Values of the aspect ratio (○) obtained by using Eq. (3) and peak amplitude (△) of the mean interface position oscillations (the right side of Fig. 3) against the control parameter. Lines are for a guide to the eye only.

These results suggest that mode suppression in the time domain could be related to the curvature effects, which necessarily rule morphological changes. Similar results were reported by Rabaud *et al.* [21] in a Saffman-Taylor instability. They showed that lateral sidebranches were generated in a finger as a response of the system due to the application of an external periodic excitation. Effects of this perturbation were amplified at low frequency values and suppressed for larger ones. They argued that amplitude damping at short wavelengths is caused by surface tension effects. Although no direct relation between the printer's instability and the Saffman-Taylor problem has been developed yet, the results of Rabaud *et al.* [21] reinforce our argument that surface tension could be crucial for the observed suppression of the oscillations we observed at higher frequencies.

IV. PATTERN SELECTION DYNAMICS

A. Transient regime of pattern growth

Pattern dynamics were observed by following in time the evolution of the spatial spectra. Time dependence of the wave vector with the highest amplitude clearly shows that a transient regime is established soon after the cylinder is

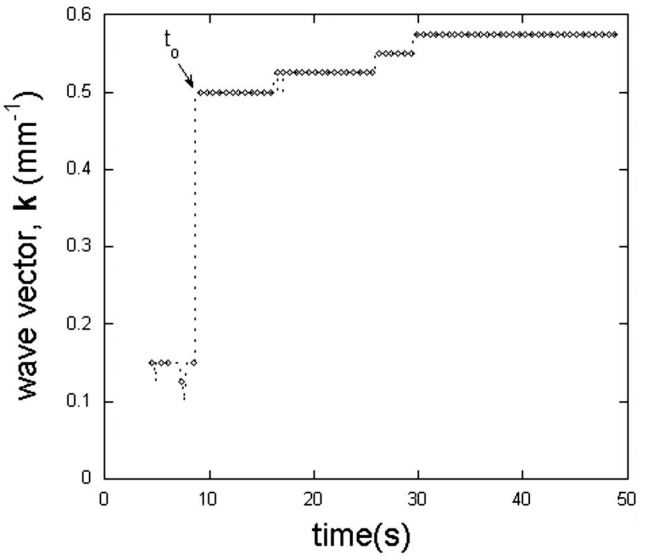

FIG. 7. k-mode evolution of spatial pattern. In the time t_0 the wave vector referent to the emerging pattern, for $b_0=300$ μm and $\xi=0.21$, appears.

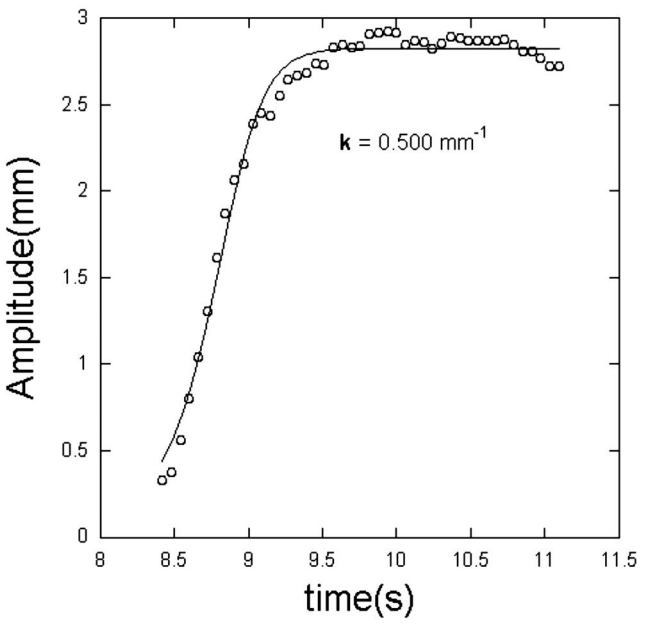

FIG. 8. Spatial mode evolution for the initial history of the spatial pattern mode with wave vector $\mathbf{k}=0.500$ mm^{-1} for $b_0=300$ μm and $\xi=0.21$.

turned on, indicating that there exists a mechanism of pattern selection in this system, even in the early stage of pattern evolution. A typical data showing this process for an experiment with $b_0=300$ μm and $\xi=0.21$ is displayed in Fig. 7. Once the selected pattern is known, it is possible to monitor in time the evolution of its amplitude. As a whole, our data suggest that the initial evolution of the pattern, in the transient regime, shows a universal profile, common to all cylinder frequencies and all mean distances b_0. Then the amplitude tends to stabilize but may present in this regime a rich dynamics. In fact, an after-transient richness in the pattern dynamics of this system has been reported in several works [4–6,8,9,11]. We show in Fig. 8, data displaying the simplest evolving pattern, presenting a quasistationary amplitude after the initial transient regime.

The linear stability analysis [7] for this problem predicts an exponential growth for the unstable spatial modes. The evolution that appears later, in the early stages of the nonlinear regime, may be described by a weak nonlinear analysis (WNL). No theory has been developed for this problem in this regime yet. For some pattern-forming problems such as directional solidification [22,23] and shallow wake flows [24], the WNL predicts a Ginzburg-Landau equation (GLE) for modes with wave vector $\mathbf{k}$, valid for sufficiently small values of the control parameter

$$\frac{dA_k}{dt} = \lambda(k)A_k - \sigma(k)|A_k|^2 A_k, \tag{4}$$

where $\lambda(k)$ is the linear growth rate and $\sigma(k)$ is the weak nonlinear coefficient. This equation admits a closed analytical solution given by

$$A_k(t) = \frac{1}{\sqrt{\frac{\sigma}{\lambda} - \left(\frac{\sigma}{\lambda} - \frac{1}{A_0^2}\right)e^{-2\lambda t}}}, \tag{5}$$

which describes the transient regime of pattern evolution. Direct observation of the WNL in the context of pattern formation was made by Figueiredo *et al.* [25] on the directional growing of a nematic-isotropic interface of a thermotropic liquid crystal. They were able to obtain both parameters (λ and σ) by adjusting their experimental curves to Eq. (5). The same procedure was applied in this work, although it is not clear that Eq. (4) is fully satisfied considering the existence of eccentricity effects in our system.

We have verified that our data fit very well to the solution of GLE in the transient regime. However, the obtained values for the linear growth rate may include some perturbation effects. For the cases $b_0=300$ μm and $b_0=400$ μm, and at large velocities, the observed GLE growth rates are greater than cylinder frequencies. Thus, pattern dynamics is faster than the characteristic time of the perturbation. This justifies a good agreement with the transient regime of the GLE. For the less unstable case, $b_0=800$ μm, we got in almost all cases, a GLE growth rate smaller than cylinder frequency but still presenting a satisfactory fit to the GLE transient regime. This effect is also expected because, as shown in Fig. 3, eccentricity has a small influence on the postbifurcation branch for this value of b_0. We solved numerically a modified version of GLE, given by

$$\frac{dA_k}{dt} = [\lambda(k) + \epsilon \sin(\omega t)]A_k - \sigma(k)|A_k|^2 A_k, \tag{6}$$

and assumed as a candidate to describe the effects of eccentricity on pattern dynamics. Results of these simulations confirm our observations in all distances b_0 configured in the experiments, showing the absence of oscillations when the pattern is in its growth phase. Thus it appears that the observed transient regime is compatible with the imposed time-dependent perturbation. Adjusted values for the linear growth rate λ_{GL}, obtained from fitting our data to the GLE,

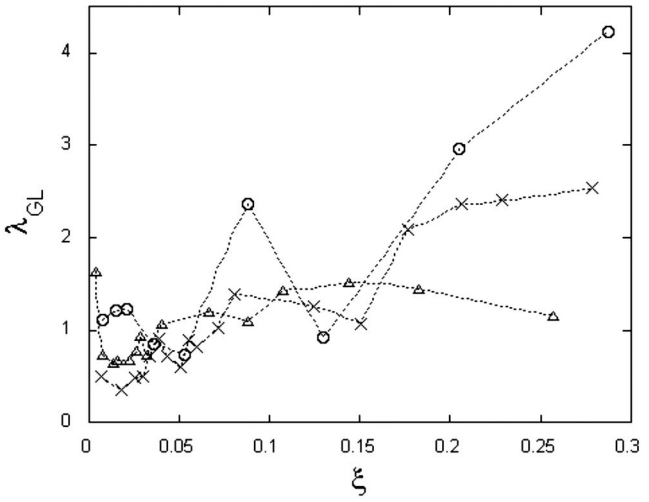

FIG. 9. Values of pattern growth rate are plotted against the control parameter for the three distances used [b_0=300 μm (○), b_0=400 μm (△), b_0=800 μm (×)]. Lines are for a guide to the eye only.

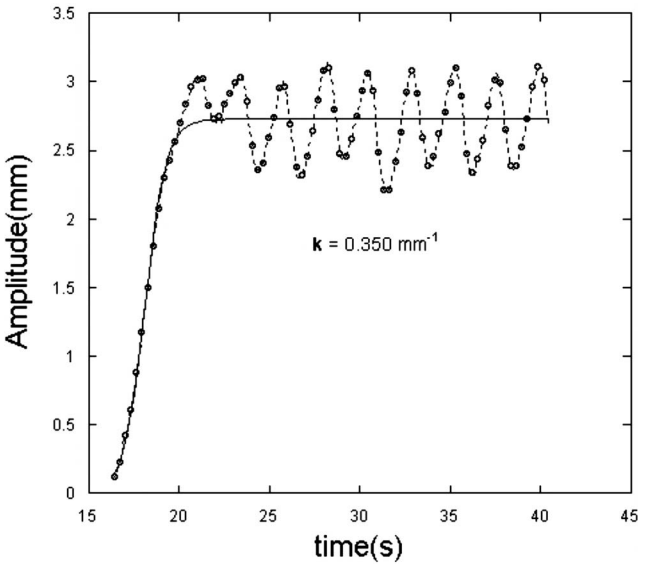

FIG. 10. A Ginzburg-Landau equation models the amplitude of pattern growth. Its nonlinear term gives its saturation value. The oscillatory mode present in the amplitude comes from changes in the pattern morphology due to the perturbation.

are plotted in Fig. 9. Our attempt to fit these values to the predicted ones by the linear stability analysis performed by Hakim *et al.* failed to obtain realistic parameters for the experiment, even for very low values of the control parameter, where this analysis is expected to be valid. Nevertheless, a concave profile for the dispersion relation, predicted by this linear theory was reached for all distances b_0. This may indicate that the perturbation really affected growth rate values still sustaining the overall transient profile predicted by the GLE.

In the saturated regime, where a GLE approach predicts a stationary pattern, we have observed an oscillatory amplitude (with the same period as the cylinder) superimposed to a constant saturation value, as displayed in Fig. 10. The same kind of profile is displayed by the numerical solutions of Eq. (6). This reinforces its validity as a candidate to analyze the transient pattern. However, our attempts to fit its solutions to the more complex pattern dynamics in the saturated regime were not satisfactory mainly due to phase mismatching between the experimental data and the obtained numerical solutions. Therefore this modified GLE gives only a general qualitative approach to the description of the perturbed pattern in the saturated regime.

As already discussed in Sec. III, oscillations in the mean interface position persist in the postbifurcation regime due to asymmetries that occur in the crests and valleys of the formed pattern. An immediate consequence of this morphological effect is oscillations in the amplitude of the spatial Fourier modes. Time-domain Fourier analysis of both types of oscillations was performed. All these spectra show a strong peak at the cylinder frequency. Interestingly, these peak amplitudes are not correlated in a simple way. Table II displays values of Pearson's correlation coefficient between those two sets of data for each b_0. It also contains, for each b_0, the ratio $\langle A_k \rangle / \langle \Delta x \rangle$ of their mean values, these averages being calculated over the whole range of control parameters. It is clear that, in the most critical case of b_0=300 μm, spatial mode oscillations almost follow the mean interface position oscillations. For the largest b_0, the ratio of the oscillations had the smallest value and a negative correlation coefficient was found. In one way this confirms that perturbation effects, in this case, have minor influence on pattern dynamics but the calculated correlation coefficient indicates that they still favor the presence of morphological asymmetries. These results suggest that coupling of the perturbation to the intrinsic pattern dynamics of this system cannot be simply related to the properties of its unstable branch, mainly determined by the value of b_0. Therefore a better theoretical comprehension of this system in the nonlinear regime, including its perturbed version, seems to be necessary in order to capture its complex pattern structure.

B. Spatial modes competition and morphological changes in the periodic pattern

This section concerns our observations of the competition among the relevant spatial modes present at different stages of pattern evolution. Measurements of the Fourier amplitude for the dominant mode (maximum amplitude mode in the spectrum), in both the initial and final stages of pattern his-

TABLE II. Values referent to the oscillation ratio between pattern amplitude ($\langle A_k \rangle$) and mean interface position ($\langle \Delta x \rangle$) averaged over all control parameters for each b_0 adjusted and the correspondent correlation coefficients.

Distance b_0 (μm)	Correlation	Mean oscillation ratio
300	0.90	0.85
400	0.16	0.29
800	−0.30	0.20

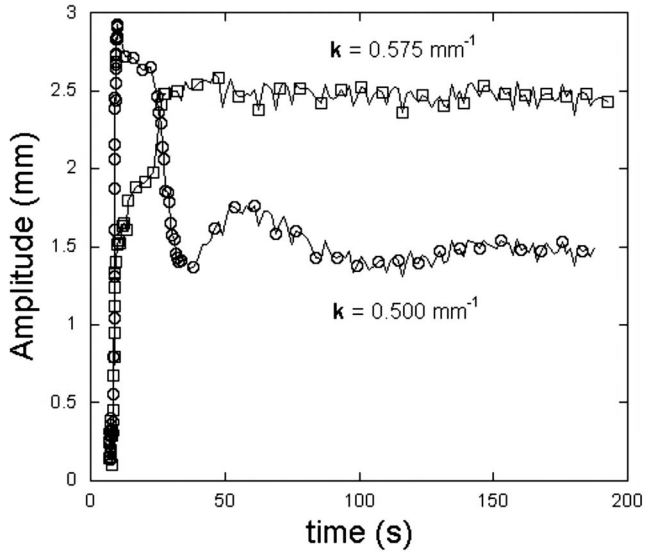

FIG. 11. Time evolution of the dominant modes [$\mathbf{k}=0.500\ \mathrm{mm}^{-1}$ (○) and $\mathbf{k}=0.575\ \mathrm{mm}^{-1}$ (□)] for $b_0=300\ \mu$m and $\xi=0.21$. Lines are for a guide to the eye only.

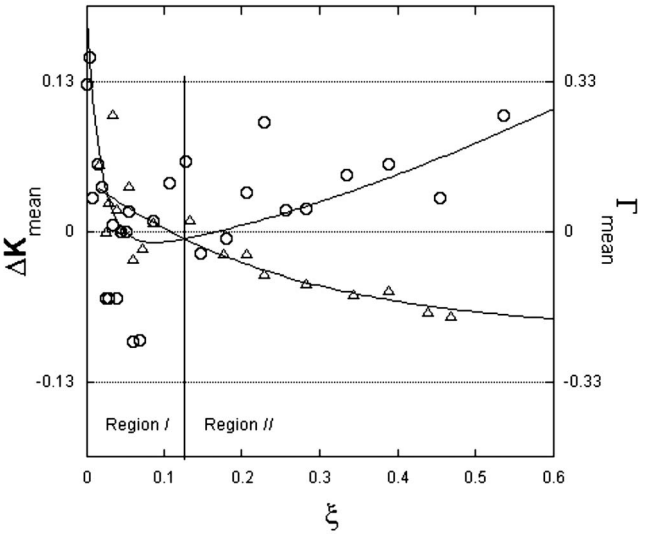

FIG. 12. Mean aspect ratio (△) and mean wave vector difference (○) of the selected patterns for the three sets of experiments realized.

tory, indicate that two different modes may share this property. These two dominant modes present a transient exponential growth in their early stages of evolution. However, for large time values compared to the characteristic time scale that defines the transient growth, the amplitude of the initial dominant mode decreases. Meanwhile, the second mode evolves and reaches a mean saturation value. Both modes are consistently described by a Ginzburg-Landau equation [Eq. (4)] in the transient regime. We checked that the second mode has a growth rate half of the first one. Figure 11 shows a typical evolution of these two modes. A switching of the amplitudes between these two dominant modes is clear and occurs at $t=25$ s. From this point, the second mode becomes dominant. Using an expression similar to Eq. (3), we calculated the normalized difference $\Delta\mathbf{k}$ of them for each control parameter and each distance b_0 selected. Then, having set the control parameter, we averaged their values over the whole set of b_0 settings. This procedure revealed a general trend for this number, which was contrasted with the average values of the aspect ratio Γ obtained from Sec. III, here averaged over the set of b_0 values. This way it was possible to confront morphological changes in the pattern with the emergence of competition modes, as the control parameter is varied. In order to display the trend of these data we fit them to two functions as follows. The set of $\Delta\mathbf{k}_{mean}$ values was adjusted using

$$a + b\ \exp(-c\xi) + d\xi^{1.5}, \tag{7}$$

and the set of Γ_{mean} values was adjusted by

$$a + b\ \exp[c(\xi - d)]. \tag{8}$$

We show in Fig. 12 the set of measured data and the adjusted curves corresponding to these equations. This picture shows the existence of two distinct regions with clear qualitative differences. For low values of the control parameter, in the region assigned as *I*, the value of $\Delta\mathbf{k}_{mean}$ roughly decreases as the control parameter increases. Values of Γ_{mean} are positive for almost all the values of the control parameter. Concerning pattern selection effects, this region has a subregion, close to the bifurcation, where wave vector values show great dispersion. This is followed by an interval (0.04,0.13) of the control parameter revealing a strong pattern selection with almost no difference between the initial and final wave vector. Simultaneously, a qualitative change in the aspect ratio is observed, with a significant dispersion in its values. When the control parameter is high (region II), the dispersion in the wave vector values increases monotonically. Thus it seems that not only does the sign crossover in the aspect ratio coincide with the interval of strong pattern selection, but also processes having large values of $\Delta\mathbf{k}_{mean}$ may present quite different asymmetrical forms.

Statistical dispersion of the data displayed in Fig. 12 is shown in Table III. This table also contains values of the Pearson correlation coefficient between the set of $\Delta\mathbf{k}_{mean}$ and Γ_{mean} data calculated for each region. We found that the obtained values for this coefficient have opposite signs. Values inside the parentheses were calculated using curve fitting

TABLE III. Statistical values comparing morphology of the interfacial front and pattern selection. $\Delta\mathbf{k}_{mean}$ is the average of the normalized wave vector difference for a specific region and $\sigma_{\Delta\mathbf{k}_{mean}}$ is its correspondent standard deviation. Γ_{mean} is the average aspect ratio for a specific region and $\sigma_{\Gamma_{mean}}$ is the standard deviation for this measurement.

Quantity	Region I	Region II
$\Delta\mathbf{k}_{mean}$	0.04(0.02)	0.06 (0.07)
$\sigma_{\Delta\mathbf{k}_{mean}}$	0.13(0.06)	0.05 (0.05)
Γ_{mean}	0.03(0.04)	−0.09 (−0.14)
$\sigma_{\Gamma_{mean}}$	0.08(0.03)	0.08 (0.05)
Correlation coefficient	0.67(0.80)	−0.20 (−0.94)

data from Eqs. (7) and (8). They confirm the general trend displayed by the experimental data and, in particular, reveal a marked change in the correlation coefficient. It becomes apparent that statistical properties of pattern morphology and pattern selection processes may be closely related. So far no theoretical model describing this system under such strong nonequilibrium conditions has been developed. Thus, our measurements can only provide a descriptive scenario.

V. CONCLUSION

We report results of an experimental study on pattern formation in a one-dimensional interfacial front. This pattern was subject to a deterministic perturbation due to an eccentricity in the cylinder used. The ensuing effects of this controlled perturbation generated a precursor mode in this system. We studied the association between this perturbation in the postbifurcation branch and the periodic spatial modes developed there. Studies made on the morphology of these patterns suggest that the instability induced by the eccentricity affects the complex time-dependent dynamics of the patterns formed. Therefore our results call for a modified amplitude equation for predicting the evolution of spatial modes of the pattern in the perturbed case. From this study, it becomes evident that statistical tools are valuable in the analysis of the interaction between morphology and dynamics of patterns found in this complex system.

ACKNOWLEDGMENTS

This work was partially supported by Brazilian Agencies CNPq and Finep-Pronex.

[1] P. Coullet and G. Iooss, Phys. Rev. Lett. **64**, 866 (1990).
[2] E. Pitts and J. Greiller, J. Fluid Mech. **11**, 33 (1961).
[3] G. I. Taylor, J. Fluid Mech. **16**, 595 (1963).
[4] M. Rabaud, S. Michalland, and Y. Couder, Phys. Rev. Lett. **64**, 184 (1990).
[5] M. Rabaud, Y. Couder, and S. Michalland, Eur. J. Mech. B/Fluids **10**, 253 (1991).
[6] L. Bellon, L. Fourtune, V. T. Minassian, and M. Rabaud, Phys. Rev. E **58**, 565 (1998).
[7] V. Hakim, M. Rabaud, H. Thomé, and Y. Couder, in *Proceedings of a NATO Advanced Research Workshop: New Trends in Nonlinear Dynamics and Pattern Forming Phenomena: The Geometry of Nonequilibrium*, edited by P. Coullet and P. Huerre (Plenum, New York, 1990), p. 237.
[8] L. Pan and J. R. deBruyn, Phys. Rev. Lett. **70**, 1791 (1993).
[9] L. Pan and J. R. deBruyn, Phys. Rev. E **49**, 483 (1994).
[10] S. Michalland, M. Rabaud, and Y. Couder, J. Fluid Mech. **312**, 125 (1996).
[11] H. Z. Cummins, L. Fourtune, and M. Rabaud, Phys. Rev. E **47**, 1727 (1993).
[12] S. Michalland and M. Rabaud, Physica D **61**, 197 (1992).
[13] L. Fourtune, W.-J. Rappel, and M. Rabaud, Phys. Rev. E **49**, R3576 (1994).
[14] R. L. Santos and J. M. A. Figueiredo, Phys. Rev. E **74**, 041104 (2006).
[15] R. C. Gonzales and R. E. Woods, *Digital Image Processing*, 2nd ed. (Pearson Education, Delhi, 2002).
[16] *Evaluation of Proposed Earthquake Precursors*, edited by M. Wyss (American Geophysical Union, Washington, D.C., 1991).
[17] K. Eftaxias, P. Kapiris, J. Polygiannakis, A. Peratzakis, J. Kopanas, G. Antonopoulos, and D. Rigas, Nat. Hazards Earth Syst. Sci. **3**, 217 (2003).
[18] J. Martinerie, C. Adam, M. Le Van Quyen, M. Baulac, S. Clemenceau, B. Renault, and F. J. Varela, Nat. Med. **4**, 1173 (1998).
[19] K. Lehnertz and C. E. Elger, Phys. Rev. Lett. **80**, 5019 (1998).
[20] K. Wiesenfeld, J. Stat. Phys. **38**, 1071 (1985).
[21] M. Rabaud, Y. Couder, and N. Gerard, Phys. Rev. A **37**, 935 (1988).
[22] D. J. Wollkind and L. A. Segel, Philos. Trans. R. Soc. London **268**, 351 (1970).
[23] B. Caroli, C. Caroli, and B. Roulet, J. Phys. **43**, 1767 (1982).
[24] A. A. Kolyshkin and M. S. Ghidaoui, J. Fluid Mech. **494**, 355 (2003).
[25] J. M. A. Figueiredo, M. B. L. Santos, L. O. Ladeira, and O. N. Mesquita, Phys. Rev. Lett. **71**, 4397 (1993).